NASA Technical Memorandum 112853

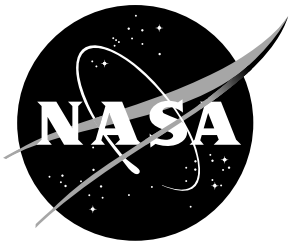

Predicting NonInertial Effects With Algebraic Stress Models Which Account for Dissipation Rate Anisotropies

T. Jongen and L. Machiels
Swiss Federal Institute of Technology, Lausanne, Switzerland

T. B. Gatski
Langley Research Center, Hampton, Virginia

May 1997

National Aeronautics and
Space Administration
Langley Research Center
Hampton, Virginia 23681-0001

Predicting NonInertial Effects With Algebraic Stress Models Which Account For Dissipation Rate Anisotropies

T. Jongen and L. Machiels
Fluid Mechanics Laboratory
Swiss Federal Institute of Technology, 1015 Lausanne, Switzerland

T. B. Gatski
Aerodynamic and Acoustic Methods Branch
NASA Langley Research Center, Hampton, VA 23681-0001, USA

ABSTRACT

Three types of turbulence models which account for rotational effects in noninertial frames of reference are evaluated for the case of incompressible, fully developed rotating turbulent channel flow. The different types of models are a Coriolis-modified eddy-viscosity model, a realizable algebraic stress model, and an algebraic stress model which accounts for dissipation rate anisotropies. A direct numerical simulation of a rotating channel flow is used for the turbulent model validation. This simulation differs from previous studies in that significantly higher rotation numbers are investigated. Flows at these higher rotation numbers are characterized by a relaminarization on the cyclonic or suction side of the channel, and a linear velocity profile on the anticyclonic or pressure side of the channel. The predictive performance of the three types of models are examined in detail, and formulation deficiencies are identified which cause poor predictive performance for some of the models. Criteria are identified which allow for accurate prediction of such flows by algebraic stress models and their corresponding Reynolds stress formulations.

I INTRODUCTION

Turbulent flows in noninertial reference frames are of considerable interest in a variety of industrial applications. However, the success of a computational analysis of such flow phenomena relies heavily on the choice of turbulence model. It is well-known that, without some modifications, conventional isotropic eddy-viscosity models fail to predict the effect of noninertial forces on turbulence, whereas second-moment closures, for example, can account for noninertial effects in a systematic way.

An explicit algebraic stress model (EASM) has been developed by Gatski and Speziale (1993) which is a nonlinear extension to an isotropic eddy-viscosity two-equation model. This EASM allows for the inclusion of stress anisotropies and rotation rate effects and is developed on a rigorous mathematical basis, while still keeping the associated computational cost comparable to that of two-equation models. Previous results have shown that this approach is a viable approximation to the full Reynolds stress closure for a variety of engineering flows. An extension to this EASM which accounts for dissipation rate anisotropies in a systematic way and is applicable to wall-bounded flows, has been recently evaluated (Xu and Speziale 1996), and is

based on an analysis of the exact transport equation for the dissipation rate tensor (Speziale and Gatski 1997). This composite algebraic stress model (CASM) is extended here to include noninertial effects in the determination of both the stress and dissipation rate anisotropies. The composite model differs from previously proposed algebraic stress models in two ways: dissipation rate anisotropies are accounted for in the constitutive relation and the coefficient of the production term in the transport equation for the scalar dissipation rate is now sensitized to the mean strain and rotation rate tensors.

The objective of this study is to systematically explore the predictive capabilities of explicit algebraic stress models in general and, in particular, the composite model for the case of a fully developed turbulent channel flow with strong spanwise rotation. This effort is an extension of previous work in that (1) the recent DNS obtained by Lamballais *et al.* (1996) has yielded new data for rotation numbers that are higher than those for the previous DNS study of Kristoffersen and Andersson (1993) (as well as the previous experimental study of Johnston *et al.*1972) and (2) the equations are integrated up to the wall, whereas most of the previous computations were limited to wall-function boundary conditions that are not suitable for (strongly) rotating flows where regions of relaminarization can occur.

II TURBULENCE MODELS

The incompressible, fully developed rotating channel flow is a unidirectional flow that results in simplified expressions for the mean flow in the noninertial frame. In this frame, the mean strain rate and rotation rate tensors

$$S_{ij} = \frac{1}{2}\left(\frac{\partial \overline{u}_i}{\partial x_j} + \frac{\partial \overline{u}_j}{\partial x_i}\right), \quad \omega_{ij} = \frac{1}{2}\left(\frac{\partial \overline{u}_i}{\partial x_j} - \frac{\partial \overline{u}_j}{\partial x_i}\right) \tag{1}$$

reduce to

$$S_{ij} = \begin{pmatrix} 0 & S & 0 \\ S & 0 & 0 \\ 0 & 0 & 0 \end{pmatrix}, \quad \omega_{ij} = \begin{pmatrix} 0 & S & 0 \\ -S & 0 & 0 \\ 0 & 0 & 0 \end{pmatrix} \tag{2}$$

where $S = S(y)$ and y is the distance measured from the (bottom) wall of the channel, as shown in Figure 1.

The common feature between linear and nonlinear eddy viscosity models is both require the solution of only two transport equations; an equation for the turbulent kinetic energy K

$$\frac{\partial K}{\partial t} = \mathcal{P} - \varepsilon + D + \frac{\partial}{\partial y}\left[\left(\nu + \frac{\nu_t}{\sigma_K}\right)\frac{\partial K}{\partial y}\right] \tag{3}$$

and an equation for the turbulent dissipation rate ε

$$\frac{\partial \varepsilon}{\partial t} = C^*_{\varepsilon 1}\mathcal{P}\frac{\varepsilon}{K} - f_2 C^*_{\varepsilon 2}\frac{\varepsilon^2}{K} + E + \frac{\partial}{\partial y}\left[\left(\nu + \frac{\nu_t}{\sigma_\varepsilon}\right)\frac{\partial \varepsilon}{\partial y}\right] \tag{4}$$

where

$$\nu_t = f_\mu C_\mu K\tau, \quad \tau = K/\varepsilon, \tag{5}$$

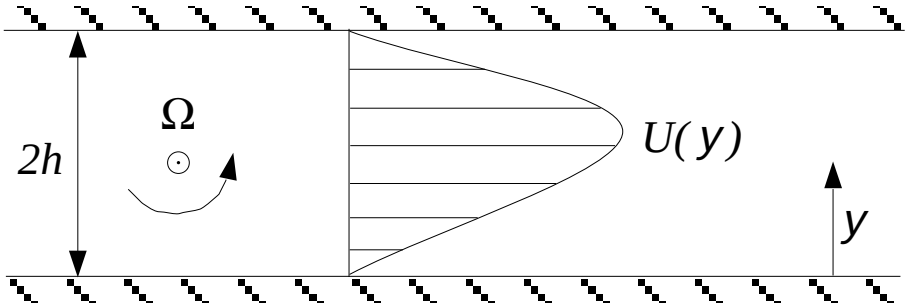

Figure 1. Schematic of fully developed turbulent channel flow in a rotating frame

$\mathcal{P} = -2\tau_{12}S$ is the turbulent production, τ_{12} is the Reynolds shear stress, f_2 and f_μ are wall damping functions, C_μ is a closure constant, and ν is the kinematic viscosity.

Three turbulence models will be evaluated by using (3) through (5): a Coriolis-modified eddy-viscosity model (EVM) proposed by Howard *et al.* (1980); , which is based on the Launder and Sharma (1974) model; a realizable algebraic stress model (ASM) (Shih *et al.* 1995); and a CASM that accounts for dissipation rate anisotropies (Xu and Speziale 1996). These three models are distinct in the way rotational effects are incorporated into their formulations.

In the EVM, the noninertial modification is phenomenological and based on an analogy with curved boundary layers. This type of modification was used recently by Pettersson *et al.* (1996) to rotating channel flow but at much lower rotation numbers. The realizable ASM model of Shih *et al.* (1995) includes the effect of mean rotation and has been tested on rotating homogeneous shear flow. The CASM is an algebraic stress model which is directly extracted from a full Reynolds stress closure as well as a transport equation for the tensor dissipation rate ε_{ij}. Thus, the model includes the effects of an anisotropic dissipation rate in a algebraic stress framework.

The Coriolis-modified eddy-viscosity model uses the Boussinesq-type relation for the Reynolds stresses:

$$b_{ij} = -f_\mu C_\mu^* \tau S_{ij}, \quad b_{ij} = \frac{\left(\tau_{ij} - \frac{2}{3}K\delta_{ij}\right)}{2K} \tag{6}$$

coupled with the relations to close (3) through (5):

$$D = -2\nu\left(\frac{\partial\sqrt{K}}{\partial y}\right)^2, \quad E = 2\nu\nu_t\left(\frac{\partial S}{\partial y}\right)^2 \tag{7}$$

$$f_\mu = \exp\left[-3.4\left(1 + \frac{Re_t}{50}\right)^{-2}\right], \quad Re_t = \frac{K^2}{\nu\varepsilon} \tag{8}$$

$$C_{\varepsilon 2}^* = \left[C_{\varepsilon 2} + 1.536S^2\tau^2\left(\frac{\Omega}{S}\right)\left(1 - \frac{\Omega}{S}\right)\right] \tag{9}$$

$$f_2 = 1 - 0.3\exp\left(-Re_t^2\right) \tag{10}$$

where $C_\mu^* = C_\mu = 0.09$, $C_{\varepsilon 1}^* = 1.44$, $C_{\varepsilon 2} = 1.92$, $\sigma_K = 1$, $\sigma_\varepsilon = 1.3$, and Ω is the rotation rate of the reference frame.

The Reynolds stress algebraic equation model (Shih *et al.* 1995) is given by

$$b_{ij} = -C_\mu^* \tau S_{ij} + c_2 \tau^2 (S_{ik} W_{kj} - W_{ik} S_{kj}) \tag{11}$$

and

$$W_{ij} \equiv \omega_{ij} + \epsilon_{mji} \Omega_m, \quad \Omega_m = (0, 0, \Omega) \tag{12}$$

where for this unidirectional shear case

$$c_2 = -\frac{\sqrt{1 - 18 C_\mu^{*2} (S\tau)^2}}{1 + 12 (S\tau)^2 \left| 1 - \dfrac{\Omega}{S} \right|}, \quad D = E = 0 \tag{13}$$

$$f_2 = \left[1 - \exp\left(-\frac{y^+}{5.5} \right) \right]^2, \quad y^+ = \frac{y u_\tau}{\nu} \tag{14}$$

$$C_\mu^* = \left[6.5 + 3\sqrt{2} |S\tau| \sqrt{1 - 3\frac{\Omega}{S} + \frac{9}{2} \left(\frac{\Omega}{S} \right)^2} \right]^{-1} \tag{15}$$

u_τ is the friction velocity, $f_\mu = 1.0$, $C_\mu = 0.09$, $C_{\varepsilon 1}^* = 1.44$, $C_{\varepsilon 2}^* = 1.92$, $\sigma_K = 1$, and $\sigma_\varepsilon = 1.3$.

The composite algebraic stress model that accounts for dissipation rate anisotropies (Xu and Speziale 1996) is a extension of the EASM of Gatski and Speziale (1993) in inertial frames. In the noninertial case, the process is complicated by the fact that the system rotation enters differently into the anisotropic dissipation rate and the algebraic stress relations.

First, noninertial effects are introduced into the explicit algebraic anisotropic dissipation rate equation developed by Speziale and Gatski (1997) as

$$d_{ij} = -\frac{2 g_\varepsilon}{15} C_{\mu\varepsilon}^* \left[\tau S_{ij} + \beta_1 \tau^2 \left(S_{ik} W_{kj}^* - W_{ik}^* S_{kj} \right) + 2 \beta_2 \tau^2 \left(S_{ik} S_{kj} - \frac{1}{3} S_{kl} S_{kl} \delta_{ij} \right) \right], \tag{16}$$

and

$$W_{ij}^* \equiv \omega_{ij} + c_\omega^* \epsilon_{mji} \Omega_m, \quad c_\omega^* = \frac{7\beta_3 + 12}{7\beta_3 + 1} \tag{17}$$

$$d_{ij} = \frac{\left(\varepsilon_{ij} - \frac{2}{3} \varepsilon \delta_{ij} \right)}{2\varepsilon} \tag{18}$$

$$C_{\mu\varepsilon}^* = \left\{ 1 - \frac{4}{3} (S\tau)^2 \left[\beta_2^2 - 3\beta_1^2 \left(1 - c_\omega^* \frac{\Omega}{S} \right)^2 \right] \right\}^{-1} \tag{19}$$

$$\beta_1 = \left(\frac{7}{11} \beta_3 + \frac{1}{11} \right) g_\varepsilon, \quad \beta_2 = \left(\frac{15}{11} \beta_3 - \frac{1}{11} \right) g_\varepsilon, \quad g_\varepsilon = \left[C_{\varepsilon 5} + \frac{\mathcal{P}}{\varepsilon} - 1 \right]^{-1} \tag{20}$$

$C_{\varepsilon 5} = 5.8$, and $\beta_3 = 0.6$.

In the absence of rotation, this explicit algebraic anisotropic dissipation rate model could be directly inserted into the explicit algebraic stress model and the resulting

composite explicit algebraic equation could be solved in conjunction with the turbulent kinetic energy and the dissipation rate equations. In the noninertial frame this direct substitution is not possible, and the problem can be quickly identified by examining the implicit relation for the algebraic stress model that is used as the starting point for the tensor polynomial expansions associated with the explicit representations. The implicit relation that accounts for dissipation rate anisotropies can be written as

$$b_{ij} + \alpha_3\tau\left(b_{ik}S_{kj} + S_{ik}b_{kj} - \frac{2}{3}b_{mn}S_{mn}\delta_{ij}\right) - \alpha_2\tau\left(b_{ik}\overline{W}_{kj} - \overline{W}_{ik}b_{kj}\right) = -\alpha_1\tau S_{ij} - gd_{ij} \tag{21}$$

and

$$\overline{W}_{ij} \equiv \omega_{ij} + \bar{c}_\omega\epsilon_{mji}\Omega_m, \quad \bar{c}_\omega = \frac{C_4 - 4}{C_4 - 2} \tag{22}$$

$$\begin{aligned} \alpha_1 &= \left(\frac{4}{3} - C_2\right)\frac{g}{2}, \quad \alpha_2 = (2 - C_4)\,\frac{g}{2} \\ \alpha_3 &= (2 - C_3)\,\frac{g}{2}, \quad g = \left[\frac{C_1}{2} + \frac{\mathcal{P}}{\varepsilon} - 1\right]^{-1} \end{aligned} \tag{23}$$

$C_1 = 3.4 + 1.8\mathcal{P}/\varepsilon$, $C_2 = 0.36$, $C_3 = 1.25$, and $C_4 = 0.40$. These constant closure coefficients are obtained from the SSG pressure-strain correlation model (Speziale *et al.* 1991). A comparison of (17) and (22) clearly shows that in general the rotation rate tensors in the noninertial frame that are extracted from the algebraic dissipation rate model and the algebraic stress model are not the same. This difference precludes a simple combination of terms as suggested by (21) and shown to be possible in inertial frames (Xu and Speziale 1996), where integrity bases were used to get a composite explicit representation for the Reynolds stresses.

As an alternative to this approach, consider (21) rewritten as the matrix system

$$\mathbf{A}\mathbf{b} = -\left(\alpha_1\tau\mathbf{s} + g\mathbf{d}\right) \tag{24}$$

where

$$\mathbf{b} = [b_{11}, b_{12}, b_{22}]^T, \quad \mathbf{s} = [0, S, 0]^T, \quad \mathbf{d} = [d_{11}, d_{12}, d_{22}]^T \tag{25}$$

$$\mathbf{A} = \begin{bmatrix} 1 & \frac{2}{3}S\tau\left(\alpha_3 + 3\alpha_2\mathcal{R}\right) & 0 \\ S\tau\left(\alpha_3 - \alpha_2\mathcal{R}\right) & 1 & S\tau\left(\alpha_3 + \alpha_2\mathcal{R}\right) \\ 0 & \frac{2}{3}S\tau\left(\alpha_3 - 3\alpha_2\mathcal{R}\right) & 1 \end{bmatrix} \tag{26}$$

$$\mathcal{R} = 1 - \bar{c}_\omega\frac{\Omega}{S} \tag{27}$$

The system in (24) can be inverted analytically to obtain explicit expressions for the Reynolds stress anisotropies b_{ij} (and τ_{ij}). Once again, these stress relations are coupled with (3) and (4) for the turbulent kinetic energy and the turbulent dissipation rate, with

$$D = E = 0, \quad f_2 = \left[1 - \exp\left(-\frac{y^+}{6.5}\right)\right]^2 \tag{28}$$

$$C^*_{\varepsilon 1} = 1 + (1+\beta)\frac{d_{12}}{b_{12}}, \quad \beta = \frac{3}{4}\left(\frac{14}{11}\beta_3 - \frac{16}{33}\right) \tag{29}$$

$f_\mu = 1.0$, $C_\mu = 0.094$, $C^*_{\varepsilon 2} = 1.83$, $\sigma_K = 1$, and $\sigma_\varepsilon = 1.3$. The additional (nonconstant) term in the expression for $C^*_{\varepsilon 1}$ represents a production ratio of the turbulent dissipation rate ($d_{12}S$) and turbulent kinetic energy ($b_{12}S$).

III RESULTS

The turbulence models presented in the last section are coupled with the streamwise momentum equation

$$\frac{\partial U}{\partial t} = -G + \frac{2}{Re_b}\frac{\partial S}{\partial y} - \frac{\partial \tau_{12}}{\partial y} \tag{30}$$

where $\overline{u}_i = (U, 0, 0)$; G is the (constant) effective pressure gradient, which includes the centrifugal force term; and the bulk Reynolds number $Re_b = hU_b/\nu$, with U_b as the bulk velocity. Equation (30), coupled with the transport equations for the turbulent kinetic energy (3) and the turbulent dissipation rate (4), is integrated to steady state by a one-dimensional second-order finite-difference scheme. This simple one-dimensional spatial problem allows for solutions with arbitrarily high numerical accuracy by using a sufficient number of points. Here, 200 points were typically used, with highly stretched meshes near the solid walls.

Because the different rotation regimes considered by the DNS (Lamballais *et al.* 1996) were obtained at the same bulk Reynolds number, the pressure gradient in the numerical code was adjusted in order to have $Re_b = 2500$ at convergence. In the following, results for three different rotation numbers, defined by

$$Ro = 2|\Omega|h/U_b \tag{31}$$

are shown ($Ro = 0$, $Ro = 0.5$, and $Ro = 1.5$). In the earlier DNS study of Kristoffersen and Andersson (1993), the maximum rotation number studied was 0.5. Thus, the DNS data used in this study significantly increases the validation range for the turbulence closure models.

The profiles of the mean velocity and turbulent kinetic energy are shown in Figures 2 and 3, respectively. The turbulent kinetic energy, as well as the turbulent stresses to be presented, are scaled by an average friction velocity u_τ, which is the half-sum of the friction velocities on both walls. The DNS results show the characteristic linear region of slope 2Ω in the mean velocity, which leads to a mean absolute vorticity $2(S - \Omega)$ that is close to zero. These results also show that the turbulent kinetic energy is higher on the anticyclonic or pressure side ($y = 0$) than on the cyclonic or suction side ($y = 2$), where relaminarization occurs. In Figure 2, for the mean velocity the composite model is able to reproduce all features of the flow for the three rotation numbers considered, including the linear portion of the profile and the relaminarization on the cyclonic side, characterized by a parabolic velocity profile. For the turbulent kinetic energy shown in Figure 3, the asymmetry of the profile and the higher turbulence intensity on the anticyclonic side of the channel are clearly visible and are consistent with the DNS results. In the case for which $Ro = 0$, the

peaks in turbulent kinetic energy near the wall are not well predicted because in the CASM no f_μ damping function has been introduced.

The Coriolis-modified model of Howard *et al.* (1980) gives reasonable predictions for the mean velocity at the different rotation numbers although not with the same degree of accuracy as the CASM. The algebraic model of Shih *et al.* (1995) does not correctly predict the mean velocity at these higher rotation numbers since it fails to predict the linear profile on the anticyclonic side and the relaminarization on the cyclonic side. For the turbulent kinetic energy, both the Howard and Shih models misrepresent the behavior of the kinetic energy in the higher rotation rate cases. At $Ro = 0.5$ and $Ro = 1.5$, the Coriolis-modified EVM yields results that effectively damp out the turbulent kinetic energy in the relaminarizing portion of the flow, whereas the Shih algebraic stress model is somewhat insensitive to the effects of rotation.

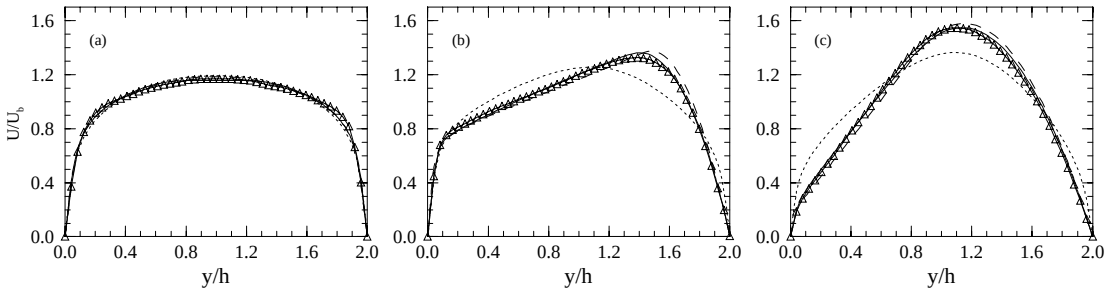

Figure 2. Mean velocity profiles for (a) $Ro = 0$, (b) $Ro = 0.5$, and (c) $Ro = 1.5$. △—△ DNS (Lamballais *et al.* 1996); ——, CASM; - - - -, ASM (Shih *et al.* 1995); – – –, Coriolis-modified EVM.

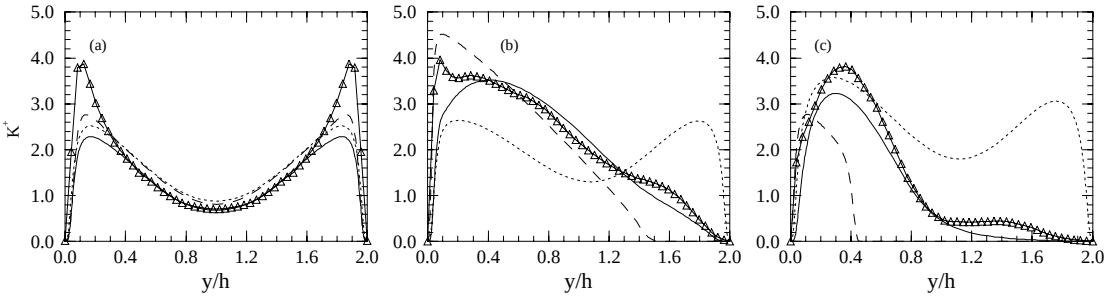

Figure 3. Turbulent kinetic energy profiles for (a) $Ro = 0$, (b) $Ro = 0.5$, and (c) $Ro = 1.5$. △—△ DNS (Lamballais *et al.* 1996); ——, CASM; - - - -, ASM (Shih *et al.* 1995); – – –, Coriolis-modified EVM.

With the success of the CASM, further investigation of the flow dynamics is worthwhile by examining the total shear stress. At steady state, (30) can be integrated

with respect to y and expressed in wall units as

$$-\tau_{12}^{+} + \frac{2}{Re_\tau} S^{+} = u_{\tau 0}^{2} \left[1 - \frac{y}{2} \left(1 + \frac{u_{\tau 2}^{2}}{u_{\tau 0}^{2}} \right) \right] \tag{32}$$

where $u_{\tau 0} = u_\tau \,|_{y=0}$, $u_{\tau 2} = u_\tau \,|_{y=2}$, and $Re_\tau = h u_\tau / \nu$. As this equation shows, the total shear must vary linearly across the channel for all rotation rates. The partition of the total shear stress between the turbulent τ_{12}^{+} and viscous $2S^{+}/Re_\tau$ stresses is illustrated in Figure 4 for the composite model. The region of neutral stability, where the velocity profile is linear, is characterized by a turbulent shear stress that varies linearly, and a viscous shear stress that remains constant.

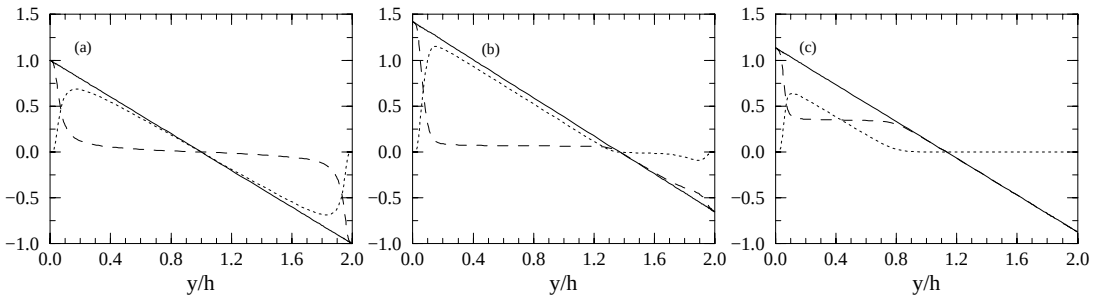

Figure 4. Partition of the total shear between turbulent and viscous shear stresses: computations by CASM for (a) $Ro = 0$, (b) $Ro = 0.5$, and (c) $Ro = 1.5$. ——, $-\tau_{12}^{+} + 2S^{+}/Re_\tau$; - - - -, $-\tau_{12}^{+}$; – – –, $2S^{+}/Re_\tau$.

In addition to the turbulent shear stress, the normal Reynolds stresses are significantly affected by the rotation. Figure 5 shows the attenuation of the normal stress components on the relaminarized side of the channel at both nonzero rotation numbers. On the turbulent side, the streamwise component τ_{11} is attenuated relative to the $Ro = 0$ case, and both the τ_{22} and τ_{33} components are enhanced relative to the $Ro = 0$ case. The most significant effect is on the τ_{22} component, but even at the high rotation case the τ_{33} component also exceeds the τ_{11} component on the anticyclonic side. This result is consistent with the DNS results and can be explained by the fact that the CASM is derived from a Reynolds stress model and will, therefore, inherit the right sensitivity of the production terms for the individual normal stresses to the rotation. On the other hand, the stress anisotropies predicted by the model of Shih *et al.* (1995) in (11) for unidirectional shear, where $b_{11} = -b_{22} = 2c_2(S\tau)^2(1 - \frac{\Omega}{S})$ and $b_{33} = 0$, show that this coupling of the b_{11} and b_{22} forces the incorrect prediction of isotropic turbulence when $\Omega = S$, and which would preclude the correct prediction of the normal stresses as displayed in Figure 5.

Both the presence of the linear velocity profile and the relaminarization process

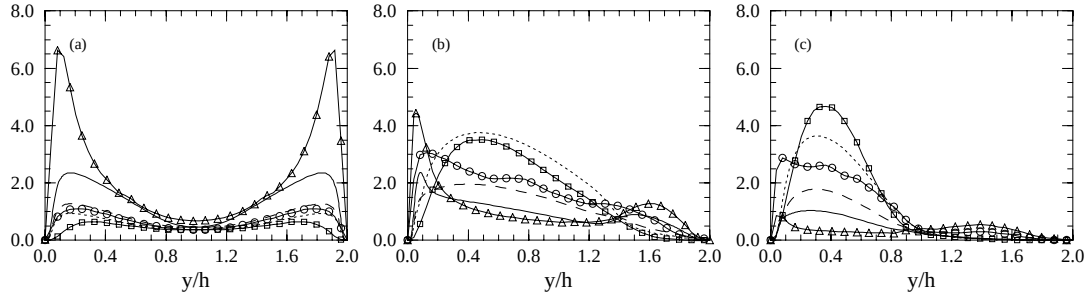

Figure 5. Turbulent normal stress profiles for (a) $Ro = 0$, (b) $Ro = 0.5$, and (c) $Ro = 1.5$. DNS (Lamballais *et al.* 1996) data: △——△, τ_{11}; □——□, τ_{22}; ○——○, τ_{33}. CASM: ——, τ_{11} - - - -, τ_{22}; – – –, τ_{33}.

can be explained. The CASM is derivable from the Reynolds stress model

$$\dot{\tau}_{ij} \; -\frac{\tau_{ij}}{K}\dot{K} - \left(\bar{\mathcal{D}}_{ij} - \frac{\tau_{ij}}{K}\bar{\mathcal{D}}_K\right) = -\frac{2\varepsilon}{g}\Bigg[b_{ij} + \alpha_3\tau\left(b_{ik}S_{kj} + S_{ik}b_{kj} - \frac{2}{3}b_{mn}S_{mn}\delta_{ij}\right) - \alpha_2\tau\left(b_{ik}\overline{W}_{kj} - \overline{W}_{ik}b_{kj}\right) + \alpha_1\tau S_{ij} + gd_{ij}\Bigg] \tag{33}$$

where $\bar{\mathcal{D}}_{ij}$ (and $\bar{\mathcal{D}}_K = \bar{\mathcal{D}}_{jj}/2$) represent the effects of turbulent and viscous diffusion; α_1, α_2, α_3, and g are given in (23). The implicit form of the algebraic stress model is obtained by setting the left side of (33) to zero and using the appropriate closure model for the dissipation rate anisotropies (such as the one shown in (16), which is used here). Note that the equilibrium hypothesis that underlies the algebraic stress models is exactly satisfied here ($\dot{\tau}_{ij} = \dot{K} = 0$), and the only approximation that is made is $\bar{\mathcal{D}}_{ij} = \frac{\tau_{ij}}{K}\bar{\mathcal{D}}_K$.

An examination of (33) shows that the anisotropy component b_{12} must satisfy the following equation:

$$0 = b_{12}\left[1 - \frac{4}{3}\alpha_3^2(S\tau)^2 + 4\alpha_2^2(S\tau)^2\mathcal{R}^2\right] + \bar{\alpha}_1 S\tau \tag{34}$$

where $\mathcal{R}$ is given in (27), and

$$\bar{\alpha}_1 = \alpha_1 + g\left[\frac{d_{12}}{S\tau} + \alpha_3(d_{11} + d_{22}) - \alpha_2\mathcal{R}(d_{11} - d_{22})\right] \tag{35}$$

As could be expected, this expression for b_{12} has the same functional form as the EASM:

$$b_{12} = -\bar{\alpha}_1\mathcal{C}_\mu^* S\tau, \quad \mathcal{C}_\mu^* = \left[1 - \frac{4}{3}(S\tau)^2\left(\alpha_3^2 - 3\alpha_2^2\mathcal{R}^2\right)\right]^{-1} \tag{36}$$

Thus, in both the composite model and the EASM the production-to-dissipation rate ratio is *always* given by

$$\frac{\mathcal{P}}{\varepsilon} \equiv -4b_{12}S\tau = 4\bar{\alpha}_1\mathcal{C}_\mu^*(S\tau)^2 \tag{37}$$

showing that $\frac{\mathcal{P}}{\varepsilon}$ is a function of both Ω/S and $S\tau$. By interchanging this dependency, the behavior of Ω/S as a function of $\frac{\mathcal{P}}{\varepsilon}$ and $S\tau$,

$$\frac{\Omega}{S} = \frac{1}{\bar{c}_\omega}\left[1 \pm \frac{1}{\alpha_2}\sqrt{\bar{\alpha}_1\left(\frac{\mathcal{P}}{\varepsilon}\right)^{-1} + \frac{1}{3}\alpha_3^2 - \frac{1}{4(S\tau)^2}}\right] \tag{38}$$

can be studied. For comparative purposes, a corresponding Ω/S relationship can also be obtained from an expression equivalent to (37) for the Shih *et al.* (1995) model;

$$\frac{\Omega}{S} = \frac{1}{3}\left\{1 \pm \sqrt{\left[\frac{4}{3}S\tau\left(\frac{\mathcal{P}}{\varepsilon}\right)^{-1} - \frac{6.5}{3S\tau}\right]^2 - 1}\right\} \tag{39}$$

Figure 6 shows the evolution of Ω/S across the channel for the different rotation regimes and the three models considered. For the two rotating cases, several features are apparent. Starting from values near zero on the anticyclonic side (because S is high near the wall), the DNS results clearly show a plateau at $\Omega/S = 1$, then quickly grow and change sign at the location of the maximum velocity ($S = 0$). On the cyclonic side, $\Omega/S\,(< 0)$ then approaches zero with a y^{-1} behavior ($S \sim -y$ in the relaminarized region). The figure shows that the CASM closely follows the DNS results and accurately predicts the location of maximum velocity. With (38),

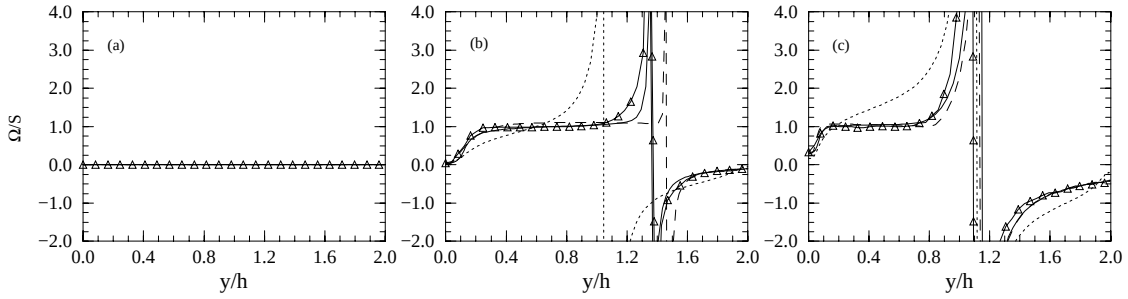

Figure 6. Scaled rotation rate variation across channel for (a) $Ro = 0$, (b) $Ro = 0.5$, and (c) $Ro = 1.5$. △——△ DNS (Lamballais *et al.* 1996); ——, CASM; - - - -, ASM (Shih *et al.* 1995); – – –, Coriolis-modified EVM.

we can explain why the CASM model is able to predict such features, and we shall see that the reason is closely related to the expression for $\mathcal{C}_\mu^*$, which must show the correct dependency on Ω/S and $S\tau$. By their nature, the CASM, and more generally, all of the algebraic stress models that are consistently derived from Reynolds stress models inherit the correct behavior for $\mathcal{C}_\mu^*$, while algebraic stress models that provide a $\mathcal{C}_\mu^*$ expression based solely on constraints such as realizability, calibrations, and phenomenological arguments *may not* have the correct behavior and will fail to predict the neutral stability region and the relaminarized zone that is observed in the rotating channel.

For larger values of $S\tau$ (i.e., $\gtrsim 3$), the last term under the root in (38) is negligible compared with the other terms, and Ω/S becomes a function of $\frac{\mathcal{P}}{\varepsilon}$ only, and takes

values on the two limit branches that correspond to the sign of $S(=\pm|S|)$. Now, it is also easy to verify that these two values of Ω/S rapidly become independent of an increasing $\frac{\mathcal{P}}{\varepsilon}$, and asymptote to either $(\Omega/S)^+$ $(S>0)$ or $(\Omega/S)^-$ $(S<0)$. Equation (38), therefore, shows that for a wide range of values of $S\tau$ and $\frac{\mathcal{P}}{\varepsilon}$ the value of Ω/S becomes effectively *independent* of these parameters, and takes values close to $(\Omega/S)^{\pm}$. These two limiting values only depend on the values of the model coefficients α_i's, and have the following values for the SSG pressure-strain model: $(\Omega/S)^+ = 0.992$ and $(\Omega/S)^- = -0.103$. In the channel away from the walls, the diffusion of K may be expected to be small, and we should have $\frac{\mathcal{P}}{\varepsilon} \approx 1$ and $S\tau \gtrsim 3$. In this case, the scaled rotation rate will have values on the limit branches that will be close to the limit values $(\Omega/S)^{\pm}$.

Figure 7 illustrates this phenomenon by showing the evolution of the scaled rotation rate correlated with the variation of $\frac{\mathcal{P}}{\varepsilon}$ across the channel. In Figure 7(a), the two

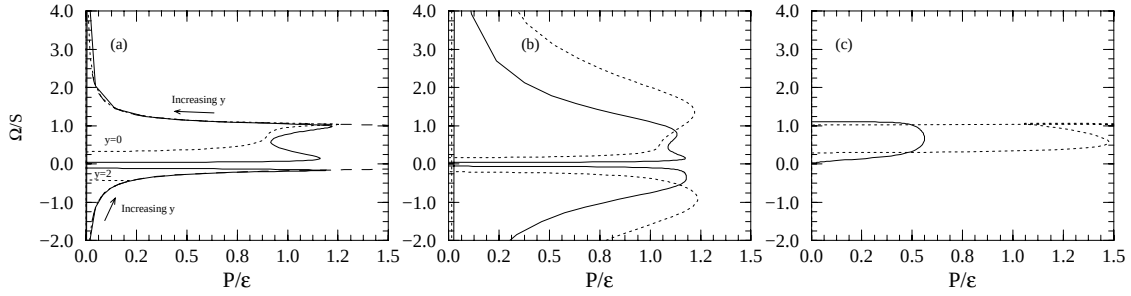

Figure 7. Scaled rotation rate variation versus $\frac{\mathcal{P}}{\varepsilon}$ in the channel for (a) CASM, (b) ASM (Shih *et al.* 1995), and (c) Coriolis-modified EVM. ——, $Ro = .5$; - - - -, $Ro = 1.5$; – – –, limit branches (shown for (a) only).

limit branches given by (38) with values of $S\tau \geq 3$ are represented by dashed lines. At $\frac{\mathcal{P}}{\varepsilon} = 0$ and $y = 0$, the curves that correspond to the CASM simulation at the two rotation regimes first move in a region where $(\Omega/S)^- < \Omega/S < (\Omega/S)^+$ because the values of $S\tau$ that are given by the model are also very small. However, as $\frac{\mathcal{P}}{\varepsilon}$ rapidly increases with movement away from the near-wall region, $S\tau$ increases also, and the points collapse on the (positive) limit branch. Until very near the wall at $y = 2$, the value of $S\tau$ stays at values sufficiently high to force the points to stay on the limit branches. After having attained values close to $(\Omega/S)^+ = 0.992$ for the major portion of the channel on the anticyclonic side, the maximum velocity point is reached, $\frac{\mathcal{P}}{\varepsilon}$ becomes very small (as $S \to 0$) and the negative limit branch is followed after the maximum velocity. For most of the values $\Omega/S < (\Omega/S)^-$, the corresponding value of $\frac{\mathcal{P}}{\varepsilon}$ on the negative branch is very small, and according to (3), we can expect $\partial K/\partial t < 0$, which leads to relaminarization in this region.

This explanation for the occurrence of the linear profile and the relaminarization process is also valid for other Reynolds stress models (i.e. other pressure-strain correlation models). For example, the LRR model (Launder *et al.* 1975) yields limiting values for Ω/S of $(\Omega/S)^+ = 0.644$ and $(\Omega/S)^- = -0.131$ for the anticyclonic and

cyclonic sides, respectively. However, one would expect that the slope of the linear velocity profile, when compared to DNS, would not be correct. Note also that these results are independent of the particular model for ε that is used, because the effect enters only through $S\tau$ and $\frac{\mathcal{P}}{\varepsilon}$.

The same analysis can be carried out on the Shih *et al.* (1995) model by using (39). With this model, the evolution of $S\tau$ always has an effect on Ω/S, and no limiting behavior occurs. Therefore, the system is then not forced to reach the asymptote $\Omega/S \approx 1$, which precludes attainment of a linear velocity profile on the anticyclonic side (Figure 7(b)). From $\frac{\mathcal{P}}{\varepsilon} = 0$ at $y = 0$, $\frac{\mathcal{P}}{\varepsilon}$ quickly increases and the resulting curve is obtained from the balance of the model equations and (39). The fact that this model cannot reproduce the correct features for the rotating channel at high rotation numbers can be attributed to the lack of a mechanism in C_μ^* to render Ω/S independent of $S\tau$ and $\frac{\mathcal{P}}{\varepsilon}$.

Finally, for the Coriolis-modified EVM, relation (37) cannot be used to find a relation between Ω/S, $\frac{\mathcal{P}}{\varepsilon}$, and $S\tau$. Instead, (4) can be examined at steady state in regions away from the walls where the damping functions and diffusive terms can be neglected. The dissipation rate equation then yields the simple relation that the production-to-dissipation rate ratio is $C_{\varepsilon 2}^*/C_{\varepsilon 1}^*$ and

$$\frac{\Omega}{S} = \frac{1}{2}\left[1 \pm \sqrt{1 - \frac{4}{1.536(S\tau)^2}\left(C_{\varepsilon 1}^* \frac{\mathcal{P}}{\varepsilon} - C_{\varepsilon 2}\right)}\right] \tag{40}$$

For sufficiently high values of $S\tau$, the dependency on $\frac{\mathcal{P}}{\varepsilon}$ is totally removed, and Ω/S takes a value of 0 or 1. Other values of Ω/S can only be reached when $\frac{\mathcal{P}}{\varepsilon}$ vanishes, as shown in Figure 7(c). Thus, the model then yields an abrupt and total damping of the turbulence. (See Figure 3.)

IV CONCLUSIONS

This study has shown that algebraic stress models consistently derived from Reynolds stress models inherit the correct dependency to rotation, and noninertial effects are automatically accounted for in a rigorous way. On the other hand, algebraic stress models that try to generalize the eddy-viscosity hypothesis in a phenomenological way are not necessarily directly extendible to non-inertial frames. As these results have shown, the nonlinear eddy-viscosity function C_μ^* must be constructed with the correct dependency on $S\tau$ and Ω/S. This study also demonstrated that the key features of the rotating channel flow were controlled by mechanisms only remotely linked to the dissipation rate equation, which would mean that phenomenological models that attempt to account for noninertial effects solely through modification of the source terms in the dissipation rate equation may not be properly accounting for essential flow physics.

Acknowledgements: The first author received support from the Commission Suisse pour l'Encouragement de la Recherche Scientifique and Sulzer Brothers S.A. under contract number 3062.1. The second author is supported by the Swiss National Foundation for Scientific Research.

V REFERENCES

Gatski, T. B., and Speziale, C. G., 1993, "On explicit algebraic stress models for complex turbulent flows," *J. Fluid Mech.*, Vol. 254, pp. 59–78.

Howard, J. H. G., Patankar, S. V., and Bordynuik, R. M., 1980, "Flow prediction in rotating ducts using Coriolis-modified turbulence models," *J. Fluid Engrg.*, Vol. 102, pp. 456–461.

Johnston, J. P., Halleen, R. M., and Lezius, D. K., 1972, "Effects of a spanwise rotation on the structure of two-dimensional fully-developed channel flow," *J. Fluid Mech.*, Vol. 56, pp. 533–558.

Kristoffersen, R., and Andersson, H. I., 1993, "Direct simulations of low-Reynolds-number turbulent flow in a rotating channel," *J. Fluid Mech.*, Vol. 256, pp. 163–197.

Lamballais, E., Lesieur, M., and Métais, O., 1996, "Effects of spanwise rotation on the stretching in transitional and turbulent channel flow," *Int. J. Heat and Fluid Flow*, Vol. 17, pp. 324–332.

Launder, B. E., and Sharma, B. I., 1974, "Application of the energy dissipation model of turbulence to the calculation of flow near a spinning disc," *Lett. Heat Mass Transfer*, Vol. 1, pp. 131–138.

Launder, B. E., Reece, G. J., and Rodi, W., 1975, "Progress in the development of a Reynolds-stress turbulence closure," *J. Fluid Mech.*, Vol. 68, pp. 537–566.

Pettersson, B. A., Andersson, H. I., and Øyulvstad, S., 1996, "Modelling system rotation with an anisotropic eddy-viscosity closure," *Proceedings of the Second ECCOMAS Conference on Numerical Methods in Engineering* , edited by J-A. Désidéri *et al.*, (Wiley Interscience, New York), pp. 683–689.

Shih, T-S., Zhu, J., and Lumley, J. L., 1995, "A new Reynolds stress algebraic equation model," *Comput. Methods Appl. Mech. Engrg.*, Vol. 125, pp. 287–302.

Speziale, C. G., and Gatski, T. B., 1997, "Analysis and modeling of anisotropies in the dissipation rate of turbulence," *J. Fluid Mech.*, to appear.

Speziale, C. G., Sarkar, S., and Gatski, T. B., 1991, "Modelling the pressure-strain correlation of turbulence: an invariant dynamical systems approach," *J. Fluid Mech.* Vol. 227, pp. 245–272.

Xu, X-H., and Speziale, C. G., 1996, "Explicit algebraic stress model of turbulence with anisotropic dissipation," *AIAA J.*, Vol. 34(10), pp. 2186–2189.